

Reconstructing the History of Structure Formation using Redshift Distortions

Yong-Seon Song and Will J. Percival

*Institute of Cosmology & Gravitation, Dennis Sciama building,
University of Portsmouth, Portsmouth, PO1 3FX, UK*

(Dated: October 27, 2018)

Measuring the statistics of galaxy peculiar velocities using redshift-space distortions is an excellent way of probing the history of structure formation. Because galaxies are expected to act as test particles within the flow of matter, this method avoids uncertainties due to an unknown galaxy density bias. We show that the parameter combination measured by redshift-space distortions, $f\sigma_8^{\text{mass}}$ provides a good test of dark energy models, even without the knowledge of bias or σ_8^{mass} required to extract f from this measurement (here f is the logarithmic derivative of the linear growth rate, and σ_8^{mass} is the root-mean-square mass fluctuation in spheres with radius $8h^{-1}\text{Mpc}$). We argue that redshift-space distortion measurements will help to determine the physics behind the cosmic acceleration, testing whether it is related to dark energy or modified gravity, and will provide an opportunity to test possible dark energy clumping or coupling between dark energy and dark matter. If we can measure galaxy bias in addition, simultaneous measurement of both the overdensity and velocity fields can be used to test the validity of equivalence principle, through the continuity equation.

PACS numbers:

I. INTRODUCTION

Observations of the accelerating nature of the Universe show that there is fundamental physics at work that we do not understand [1, 2]. Many possibilities have been postulated including a new form of the vacuum which is not present in the contemporary high energy physics, or a modification of gravity which would revolutionize our understanding of space and time. Discovering which mechanism is correct is one of the key challenges for 21st century science.

The detection of acceleration was obtained by using supernovae as standard candles, and therefore relies on measuring the cosmological geometry. The physical process causing the acceleration could also affect structure formation, which provides a complementary way of distinguishing between models. In particular, models in which general relativity is unmodified have different Large-Scale Structure (hereafter LSS) formation timescales compared with Modified Gravity (hereafter MG) models [3, 4]. Because of this, many previous studies have considered testing the signature on LSS formation predicted by MG models [5, 6, 7]. Direct observations of LSS growth as traced by galaxies are of limited value because galaxies are not expected to be simple tracers of the underlying matter density field, although we return to this point later.

Maps of galaxies where distances are measured from spectroscopic redshifts show anisotropic deviations from the true galaxy distribution. These differences arise because galaxy recession velocities include components from both the Hubble flow and peculiar velocities from the motions of galaxies in comoving space. Although these “redshift-space distortions” are a nuisance when trying to reconstruct the true distribution of galaxies, they provide a mechanism to measure the build-up of

structure, which drives these peculiar velocities on large-scales.

In linear theory, and in the absence of bias, a distant observer should expect a multiplicative enhancement of the overdensity field δ that is proportional to $1 + f\mu^2$, where f is the logarithmic derivative of the linear growth rate, and μ is the cosine of the angle to the line-of-sight [9]. With a local linear bias, the real-space galaxy density field is affected, while the peculiar velocity term is not, so the multiplicative factor is changed to $1 + \beta\mu^2$, where $\beta \equiv f/b$. Because of the μ dependence, this information can be extracted from galaxy redshift surveys, and a number of methods and their application have previously been considered. Analyses have been undertaken using the 2degree-Field Galaxy Redshift Survey (2dFGRS) [10], measuring redshift-space distortions in both the correlation function [11, 12] and power spectrum after decomposing into an orthonormal basis of spherical harmonics and spherical Bessel functions [13]. Using the Sloan Digital Sky Survey [14], an Eigenmode decomposition has been performed to separate real and redshift-space effects [15, 16]. In a recent paper, these low redshift analyses were extended to $z \simeq 1$ [17] using the VIMOS-VLT Deep Survey (VVDS) [18, 19]. In addition to measuring β at $z = 0.8$, this work has pushed explicitly the idea of using large-scale peculiar velocities for constraining models of cosmic acceleration. These data, and the resulting cosmological constraints, are considered further in Section III A. In particular we argue that it would be better to present results in terms of $b(z)\sigma_8(z)$ and $f(z)\sigma_8(z)$, rather than β for local linear bias models. We show in Section III that bias-independent constraints on $f(z)\sigma_8(z)$ are able to discriminate between some models of acceleration as well as $f(z)$, which is commonly extracted from β by applying an independent (and difficult) measurement of bias. Galaxy bias measurements tend to have the same fractional error as the redshift-

space distortion measurements: for example comparing redshift-space distortion results from the 2dFGRS[12] with bias measurements from measurements of the 3-pt function[36].

In addition to a direct measurement of $f(z)\sigma_8(z)$, redshift-space distortion measurements can be used to test diverse aspects of LSS, as proposed by Song & Koyama [8]: geometrical perturbations can be reconstructed from the evolution history of peculiar velocities. With the assumption of an additional measurement of galaxy bias, the continuity equation can be tested, and anisotropic stress can be constrained. Those diverse tests strengthen our power to constrain theoretical models, and are considered further in Section IV. Before we do this, we first review the physics that we hope to test using peculiar velocities (Section II), and then consider the measurements themselves and what they can directly tell us about structure formation (Section III).

II. LINEAR STRUCTURE FORMATION

A. Basic equations

In this section, we briefly review the standard derivation of the dynamics of the density fluctuations and their associated peculiar velocities in a Friedman universe. We will contrast this against non-standard models in later sections. In the Newtonian gauge, the perturbed metric describing local gravitational instability of the energy-momentum density fluid is given by

$$ds^2 = -(1 + 2\Psi)dt^2 + a^2(1 + 2\Phi)dx^2, \quad (1)$$

where scalar perturbations are dominant over vector or tensor perturbations. The Newtonian force Ψ sources the dynamics of the perturbed fluids, while the curvature perturbation Φ measures the local energy density fluctuations. In the epoch of non-relativistic particle domination, in standard GR models, Φ is identical to $-\Psi$, and there is no anisotropic stress.

The spatial variation of density fluctuations is expressed by the density contrast $\delta_X = \delta\rho_X(t, \mathbf{x})/\bar{\rho}_X(t)$ where X denotes the specific fluid that we are considering. In the approximation of negligible irrotational flow, the divergence of the peculiar velocity \mathbf{v}_X , $\theta_X \equiv \nabla \cdot \mathbf{v}_X$ can be used to describe the fluid motion. The dynamics of scalar perturbations of the fluid X is well described by energy momentum fluctuations δ_X and θ_X , and the corresponding metric perturbations Ψ and Φ .

The conservation equation $\nabla_\mu T_\nu^\mu = 0$ gives the set of equations that describe the dynamics of fluid X ,

$$\begin{aligned} \frac{d\delta_X}{dt} &= -(1 + w_X)\frac{\theta_X}{a} - 3H\frac{\delta p_X}{\rho_X} + 3Hw_X\delta_X, \quad (2) \\ \frac{d\theta_X}{dt} &= -H(1 - 3w_X)\theta_X - \frac{dw_X/dt}{1 + w_X}\theta_X \\ &\quad + \frac{k^2}{a} \left(\frac{\delta p_X}{\rho_X} \frac{1}{1 + w_X} - \sigma_X + \Psi \right), \quad (3) \end{aligned}$$

where w_X is the equation of state, δp_X is the perturbed pressure and σ_X is the anisotropic stress. The continuity equation, Eq. (2), states conservation of local density. The Euler equation, Eq. (3), represents the conservation of local energy momentum, and describes dynamics of perturbed fluids sourced by Ψ .

The curvature perturbation Φ is constrained to the local inhomogeneity via the Poisson equation,

$$k^2\Phi = 4\pi G_N a^2 \rho_X \left(\delta_X + 3aH\frac{\theta_X}{k^2} \right). \quad (4)$$

These equations completely determine the dynamical evolution of LSS, within a given expansion history H .

For models based on general relativity with a standard dark energy that does not clump on small scales, the scale and time dependence of the evolution of perturbations are separable in the matter dominated regime. Both δ_X and θ_X are uniquely determined by the expansion history H . Thus we are able to trace the evolution of structure formation using observations of either δ_X or θ_X in these models.

B. Dark energy model without clumping

In standard dark energy models (hereafter sDE), the cosmic expansion is accelerated by introducing a homogeneous dark energy component into the Friedman equation, which then predicts an expansion rate H ,

$$H^2 = H_0^2 \left[\frac{\Omega_b}{a^3} + \frac{\Omega_c}{a^3} + \frac{\Omega_{DE}}{a^{3(1+w_{DE})}} \right], \quad (5)$$

where ‘ b ’ denotes baryon, ‘ c ’ denotes cold dark matter.

The incoherence between baryons and CDM perturbations caused by acoustic waves in the early universe is removed at redshifts $z \gtrsim 10$ [20], and can therefore be ignored in our analysis. We also assume a negligible cosmological neutrino density, consistent with observations (e.g. [21]). Following these approximations, all matter inhomogeneities can be assumed to coherently evolve with those in the CDM. Thus we can treat all matter as a single fluid denoted by ‘ m ’. Eq. (2) and Eq. (3) for matter fluid ‘ m ’ are,

$$\frac{d\delta_m}{dt} + \frac{\theta_m}{a} = 0 \quad (6)$$

$$\frac{d\theta_m}{dt} + H\theta_m = \frac{k^2}{a}\Psi. \quad (7)$$

Since we are assuming that the dark energy is homogeneous on the scales of interest, the metric perturbations can be simply related to the total matter-energy fluctuations,

$$k^2\Phi = 4\pi G_N a^2 \rho_m \delta_m. \quad (8)$$

We use Λ CDM model as an example of sDE with the cosmological parameters $w_c(\Omega_c h^2) = 0.11$, $w_b(\Omega_b h^2) = 0.021$ and $h = 0.72$.

The combination of Eq. (8), the anisotropic stress relation $\Phi = -\Psi$, and the coupled equations of Eq. (6) and Eq. (7) provide a unique solution for the formation of cosmological structure. See [22] for a review of methods to solve these equations.

C. Modified Gravity: DGP

The cosmic acceleration may arise from a modification of gravity on cosmological scales as in the DGP model [3]. In this model, we live on the $(3+1)$ -dimensional brane which is embedded in an infinite Minkowski bulk. The weakened gravity at cosmological scales induces the cosmic acceleration without introducing dark energy. The expansion history of DGP model is determined by the usual matter-energy density and the crossover scale defined as the ratio of 5-dimensional to 4-dimensional Planck mass scales $r_c = M_{pl}^{(4)2}/2M_{pl}^{(5)3}$.

$$H^2 - \frac{H}{r_c} = \frac{8\pi G_N}{3}\rho_m. \quad (9)$$

As an example of DGP models, we take the same w_c and w_b as in our Λ CDM model discussed in section II B, but use a different $h = 0.80$ in order to provide a nearly identical $H(a)$.

In general the equations of motion of linear perturbations in DGP is not closed without solving the dynamic equation of propagation through the bulk. But in the quasi static limit $k/aH \gg 1$, where the contribution of bulk gradient is negligible, the solution can be derived from dynamic equations on the brane. In this regime, the perturbed potentials in DGP become modified,

$$k^2\Phi = 4\pi G_N \left(1 - \frac{1}{3\beta_{DGP}}\right) a^2 \rho_m \delta_m, \quad (10)$$

$$k^2\Psi = -4\pi G_N \left(1 + \frac{1}{3\beta_{DGP}}\right) a^2 \rho_m \delta_m, \quad (11)$$

where

$$\beta_{DGP} = 1 - 2r_c H \left(1 + \frac{\dot{H}}{3H^2}\right). \quad (12)$$

The effective Newtonian constant in Poisson equation $k^2\Phi = 4\pi G_{eff}(a)a^2\rho_m\delta_m$ becomes $G_{eff}(a) = G_N(1 - 1/3\beta_{DGP})$, and a non-trivial anisotropic stress is introduced

$$\frac{\Phi}{\Psi} = \frac{1 - 3\beta_{DGP}}{1 + 3\beta_{DGP}}, \quad (13)$$

while there are no changes in the continuity equation and the Euler equation [5, 23, 24].

The differences between DGP and sDE models lead to distinct evolution of δ_m and θ_m even for models with identical expansion histories. Coupling measurements of either δ_m or θ_m with observations of the geometrical evolution has the potential to distinguish DGP from sDE

models. If we are able to measure both δ_m and θ_m simultaneously, then the non-trivial anisotropic stress can be measured, which also distinguishes DGP and sDE models.

D. Dark energy model with clumping

If the dark energy can support long-lived fluctuations, then the galaxies will trace the total density fluctuations δ_T rather than those just in the matter δ_m . In these clumping dark energy models (hereafter cDE), the baryons will fall into the potential wells created by both the dark matter and energy. Given the different physical behaviour of dark matter and dark energy δ_T will not be a simple linear function of δ_m . The Poisson equation with dark energy clumping will be given by

$$k^2\Phi = 4\pi G_N a^2 \rho_T \delta_T. \quad (14)$$

where $\rho_T \delta_T = \rho_m \delta_m + \rho_{DE} \delta_{DE}$ [25].

When we have multiple components with different equations of state, the peculiar velocities of the different components will not, in general, be the same at any spatial location. Consequently, we will measure θ_m from galaxy redshift-space distortions, rather than θ_T . The continuity equation holds for matter and DE separately, although it does not hold if we mix components. So, for example,

$$\frac{d\delta_T}{dt} + \frac{\theta_m}{a} \neq 0, \quad (15)$$

in general. If we can measure δ_T and θ_m , we can distinguish between DGP and cDE by using Eq. (15). For example, if the contribution from dark energy fluctuations are accidentally identical to the effect of G_{eff} of DGP,

$$G_{eff}(a) = G_N \frac{\rho_T \delta_T}{\rho_m \delta_m}, \quad (16)$$

and the anisotropic stress causes a similar change to Ψ in Eq. (13) of DGP, then there is no difference in structure formation as measured by the evolution of θ_m . However, if we observe δ_T , then we can break the consistency of Eq. (15), leading to a possible method for distinguishing between these models.

E. Interacting dark energy model

Current observations allow a coupling between dark matter and dark energy [26, 28], although the coupling between baryon and dark energy is strongly limited by current experimental constraints [29]. For a model with interacting dark matter and dark energy (hereafter IDE),

the set of background continuity equations are,

$$\begin{aligned} \frac{d\rho_b}{dt} + 3H\rho_b &= 0 \\ \frac{d\rho_c}{dt} + 3H\rho_c &= -\gamma\rho_c \frac{d\phi}{dt} \\ \frac{d\rho_v}{dt} + 3H(\rho_v + p_v) &= \gamma\rho_c \frac{d\phi}{dt}, \end{aligned} \quad (17)$$

where γ is an arbitrary coupling constant. A positive coupling constant represents decay from dark matter to dark energy, and a negative coupling constant represents decay from dark energy to dark matter. The equation of motion of the scalar field is given by

$$\frac{d^2\phi}{dt^2} + 3H\frac{d\phi}{dt} + \frac{dV}{d\phi} = \gamma\rho_c. \quad (18)$$

The conservation equation leads to a set of dynamic equations for baryons and for dark matter. For baryons, there is no signature from the coupling in either the continuity equation or the Euler equation. For the dark matter, the coupling influences the dynamics,

$$\frac{d\delta_c}{dt} + \frac{\theta_c}{a} = 0 \quad (19)$$

$$\frac{d\theta_c}{dt} + H\theta_c - \gamma\frac{d\phi}{dt}\theta_c = \frac{k^2}{a}\Psi - a\gamma^2\rho_c\delta_c. \quad (20)$$

The continuity equation still holds because the creation/destruction rate of dark matter is proportional to its current density, but the coupling between dark matter and dark energy changes the Euler equation.

The interaction between dark matter and dark energy modifies the dynamics of dark matter, so two test particles of baryon and dark matter placed in the same force field will respond differently. There is no change in the matter continuity equation but, in general, we will measure the velocities of baryonic material, while we observe galaxies in the dark matter potential wells, so measure matter overdensities. The observed continuity equation will then be broken in the presence of coupling between dark matter and dark energy [30].

III. MEASURING PECULIAR VELOCITIES

If we map cosmological structure by translating observed galaxy redshifts to distances assuming that they are cosmological in origin then peculiar galaxy velocities are misinterpreted, leaving an anisotropic galaxy distribution. For pairs of galaxies with large separation, the peculiar velocities can tell us about the formation of large-scale structure[9]. On small scales, decoherent peculiar velocities cause Fingers-of-God (FOG), stretching compact structures along the line-of-sight. These distortions depend on the structure of halos and any cosmological information is difficult to distinguish from halo

properties. The redshift-space power spectrum $P_g^s(\mathbf{k})$ of a galaxy redshift survey is commonly modelled [9, 38] as

$$P_{gg}^s(\mathbf{k}) = [P_{gg}(\mathbf{k}) + 2\mu^2 P_{g\theta_g}(\mathbf{k}) + \mu^4 P_{\theta_g\theta_g}(\mathbf{k})] F(k^2\sigma_v^2(z)\mu^2), \quad (21)$$

where $\mu = k_{\parallel}/k$ is the cosine of the angle of the \mathbf{k} vector to the line of sight. P_g , $P_{\theta_g\theta_g}$, and $P_{g\theta_g}$ are the real space auto-power spectra of galaxies and θ_g , and the cross power spectrum of galaxy- θ_g fluctuations, respectively. σ_v and F determine the non-linear velocity distribution of galaxies in collapsed structures. It is common to assume an exponential model for the pairwise peculiar velocities, so $F(k^2\sigma_v^2(z)\mu^2) = (1 + k^2\sigma_v^2(z)\mu^2)^{-1}$, although Gaussian models have also been considered [38]. Even in the distant-observer limit, the usefulness of this equation is limited because Eq. (21) is not physically motivated [39]. Additionally, σ_v is expected to be a function of halo mass and redshift. Consequently, in order to exploit the precision available from future surveys, it may become necessary to model the exact behaviour using simulations [40, 41, 42]. In this paper, we assume that Eq. (21) holds, and that any significant deviations can be accurately modelled prior to the new data sets becoming available.

A concern is that the distribution of galaxy pair-velocities on large scales might not match the distribution of velocities in the matter field. For example, the velocity power spectrum for peaks in a density field does not match that of the mass [43, 44], even if they are the same locally. In this paper, we follow the standard ansatz that this bias is small (e.g. [7]) and assume that $\theta_g \simeq \theta$. Current simulations indicate that this might cause a 10% systematic error on scales 10–200 h Mpc⁻¹ [40, 41], although we are confident that this can be accurately simulated, so will only affect future measurements at a lower level. In the following we therefore drop the subscripts g and m from θ .

We ignore any cosmological information in $F(k^2\sigma_v^2(z)\mu^2)$, and treat this component as a “nuisance parameter” to be marginalised over, and concentrate on the cosmological information in the linear part of Eq. (21).

For linearly evolving density fields, if we can write down a linear mass conservation equation $\theta = -a\delta_m$, then the growth factor of θ , $D_\theta \propto a\dot{D}$. Defining $f \equiv d \ln D / d \ln a = \dot{D} / (DH)$, if δ_g is perfectly correlated with θ everywhere, then the power spectra in Eq. (21) have the same shape, and we have that

$$P_g^s(\mathbf{k}) = P_g(\mathbf{k}) [1 + 2\mu^2\beta + \mu^4\beta^2] F\left(\frac{k^2\mu^2\sigma_v^2}{H^2(z)}\right), \quad (22)$$

where $\beta \equiv f/b$.

Note that writing Eq. (22) in terms of β suggests that the large-scale redshift-space distortions depend on the galaxy bias. We expect the motion of galaxies to locally match those of the matter field, so two galaxies at the same location would have the same peculiar velocities irrespective of their internal properties: they simply act

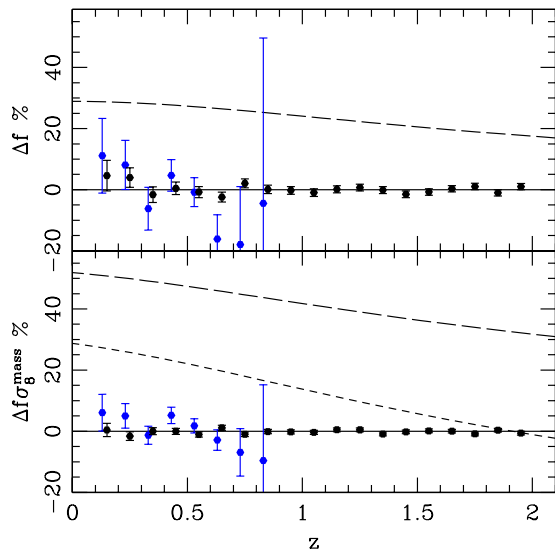


FIG. 1: The top panel shows the percentage difference in f between the sDE and DGP model (long dashed line). The sDE and DGP models are described in detail in Section III C. The background expansion has been matched between these two models. The bottom panel shows the percentage difference of $f\sigma_8^{\text{mass}}$ between sDE and DGP. Here, the long-dashed curve includes CMB data, normalising the models at the epoch of last scattering (using $\Delta_{\zeta_{\text{ini}}}^2$), while the dashed curve shows the model normalised using a low redshift measurement of $\sigma_8^{\text{mass}}(z=0) = 0.82$, matching the 5-year WMAP best-fit Λ CDM value [37]. The blue and black error bars are estimated from BOSS and EUCLID respectively (see Section III B for details).

as test particles within the matter flow. This assumption is part of Eq. (21): the dependence on bias simply comes from expecting a multiplicative correction to the observed galaxy power spectrum for the redshift-space distortions. If we instead consider modelling an additive contribution, then the dependence on bias can be broken.

Comparing Eq. (21) and (22) shows that, although many observational studies present results in terms of β , the fundamental constraint from the μ dependence of the normalisation of Eq. (21) is on the normalisation of $P_{\theta\theta}$, and the cross power $P_{g\theta}$. If we assume that the continuity equation holds, and we have a local linear bias so $\delta_g = b\delta_{\text{mass}}$, then the normalisation of P_{gg} depends on $(b\sigma_8^{\text{mass}})^2$, $P_{g\theta}$ depends on $(f\sigma_8^{\text{mass}})(b\sigma_8^{\text{mass}})$, and $P_{\theta\theta}$ depends on $(f\sigma_8^{\text{mass}})^2$. If the redshift-space distortions are modeled as a multiplicative component, then we constrain $(b\sigma_8, \beta)$, while if they are modeled as an additive component we measure $(b\sigma_8, f\sigma_8)$. These constraints will be a simple transform of each other, and should give the same likelihood surface if we transform into the same basis (this will be considered further in future work[54]). Previous analyses have, in general, converted observational results into a constraint on f using a separate measurement of bias (e.g. [17]). A perfect estimate of bias would allow us to break $f\sigma_8^{\text{mass}}$ and $b\sigma_8^{\text{mass}}$ to pro-

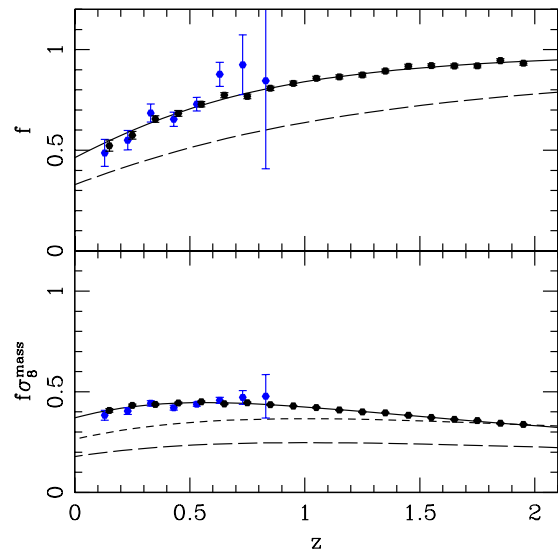


FIG. 2: The top panel shows the time evolution of f : solid curve is for sDE model, and a long-dash curve is for DGP. The sDE and DGP models are described in detail in Section III C. The bottom panel shows the evolution of $f\sigma_8^{\text{mass}}$: the solid curve shows the sDE model, the long-dash curve DGP normalised using $\Delta_{\zeta_{\text{ini}}}^2$, and the short-dashed line, DGP $\sigma_8^{\text{mass}}(z=0) = 0.82$. The blue and black error bars are estimated from BOSS and EUCLID respectively (see Section III B for details).

vide separate constraints on σ_8^{mass} , f and b . Note that f , σ_8^{mass} and b are all redshift dependent functions.

In Fig. 1 and Fig. 2, we show that the combined quantity, $f\sigma_8^{\text{mass}}$ is sufficient to distinguish between DGP and sDE models described in Section III C, if the fluctuations are additionally normalised using CMB data. If however, we normalise the model predictions for $f\sigma_8^{\text{mass}}$ using a present day measurement of σ_8^{mass} , then the predicted differences in f and $f\sigma_8^{\text{mass}}$ between the DGP and sDE models are very similar, a consequence of the weak difference in the low-redshift evolution of σ_8^{mass} . Normalising the model prediction for $f\sigma_8^{\text{mass}}$ at low redshift is a fairer comparison between using the two ways of describing the redshift-space distortion constraints, as this effectively only uses the ratios between measurements of $f\sigma_8^{\text{mass}}$ at different redshifts.

Given that no technique is significantly better at distinguishing these models in terms of the statistical error, it is worth considering the potential for including systematic errors using both techniques. Here, $f\sigma_8^{\text{mass}}$ wins, since it can be measured without knowing the bias b or the amplitude of the matter fluctuations σ_8^{mass} .

In this analysis we have compared two models of acceleration. Clearly, future measurements will be used to test a wide range of models. It is clear that for some of these f will be superior, while for others using $f\sigma_8^{\text{mass}}$ directly would provide tighter constraints. In particular, using $f\sigma_8^{\text{mass}}$ directly can be advantageous for a model such as the DGP model tested here in which growth of structure

formation is suppressed compared with Λ CDM. This is not true for other theoretical models in which growth of structure is less suppressed, e.g. normal branch DGP, compared with the self-accelerating DGP model considered here [55].

A. current constraints

Redshift-space distortions have recently been measured at $z = 0.77$ using the VIMOS-VLT Deep Survey (VVDS)[17]. They use $\sigma_8^{\text{mass}}(z = 0) = 0.78 \pm 0.03$ measured by the WMAP experiment, extrapolated to the survey redshift $z = 0.77$ $\sigma_8^{\text{mass}}(z = 0.77) = 0.54 \pm 0.03$ (assuming a fiducial $\Omega_m = 0.25, \Omega_\Lambda = 0.75$ cosmology) to measure the bias. Using this estimate, they convert their measured value of β to provide a constraint on $f(z)$. If we do not do this bias modelling, then we can reconstruct the constraint on $f\sigma_8^{\text{mass}}$ from their quoted results. To do this, we take their $f(z = 0.77) = 0.91 \pm 0.36$ measurement and multiply by the extrapolated WMAP result $\sigma_8^{\text{mass}}(z = 0.77) = 0.54$. Doing this, their redshift-space distortion measurement becomes $f\sigma_8^{\text{mass}} = 0.49 \pm 0.18$ at $z = 0.77$. We have conservatively assumed that all of the quoted error comes from the LSS observations rather than the extrapolated CMB normalisation and subsequent bias estimate.

At lower redshift, we use results from a spherical harmonics analysis of the 2dFGRS[13]. This work did not provide a direct constraint on $f\sigma_8^{\text{mass}}$ at the fiducial redshift of the 2dFGRS, but extrapolated this to $z = 0$. Without loss of generality, we can undo this extrapolation using their fiducial cosmology. For this cosmology ($\Omega_m = 0.3, \Omega_\Lambda = 0.7$), $D(z = 0.17)/D(z = 0) = 0.916$, and $f(z = 0.17)/f(z = 0) = 1.2$. Their extrapolated $z = 0$ measurement of $f\sigma_8^{\text{mass}} = 0.46 \pm 0.06$ should therefore be considered a measurement $f\sigma_8^{\text{mass}} = 0.51 \pm 0.06$ at $z = 0.17$.

We also include a measurement of redshift-space distortions from the SDSS LRG catalogue[16]. This work measured $\beta = 0.309 \pm 0.035$ at $z = 0.35$. To convert to a constraint on $f\sigma_8^{\text{mass}}$, we multiply by $b\sigma_8^{\text{mass}} = 1.43$ from the joint SDSS+CMB fit presented. Here we assume that, because of the wide survey geometry in the SDSS, the measurement error on β is significantly larger than that on $b\sigma_8^{\text{mass}}$. This gives a measurement $f\sigma_8^{\text{mass}} = 0.44 \pm 0.05$.

B. future constraints

In order to see how these constraints will improve with the next generation of experiments, we have calculated expected errors for three types of future experiment. We have considered a ground based redshift-survey of galaxies out to $z = 0.8$, based on the BOSS experiment, part of the SDSS-III (see www.sdss3.org). For this survey we have assumed that redshifts will be measured for

1.5×10^6 galaxies over $10\,000 \text{ deg}^2$ with approximately constant number density out to $z = 0.7$. We also consider a next generation space based mission that could measure 0.5×10^9 galaxies in a volume $V = 1 \times 10^{11} h^{-3} \text{ Mpc}^3$ out to $z = 2$. Such a survey is proposed has been proposed to ESA mission as part of the EUCLID mission, and is the result of the merging between SPACE and DUNE [45, 46, 47]. We have also considered the type of experiment that could be accomplished using a wide-field multi-object spectrograph on a 8m-class telescope. Here, we took the ‘‘fiducial survey’’ parameters presented for the proposed WFMOS instrument [48]. These are two surveys with number density $5 \times 10^{-4} h^3 \text{ Mpc}^{-3}$, one of 2 000 000 galaxies with $0.5 < z < 1.3$, and one of 600 000 galaxies with $2.3 < z < 3.3$. The numbers and the derived expected measurements for all of these surveys should provide an approximate guide to the improvements that are expected beyond current observations.

To calculate expected errors for these surveys, we use the fitting formula presented in [17], which was derived from numerical simulations. This formula was presented as providing the error on f , and relies on having an independent accurate measurement of σ_8^{mass} (which is itself dependent on cosmology through the growth rate, rather than its derivative). In the above discussion we argued that it is more consistent to measure and test a constraint on $f\sigma_8^{\text{mass}}$, and we translate the [17] formula as giving a fractional error

$$\frac{\Delta(f\sigma_8^{\text{mass}})}{f\sigma_8^{\text{mass}}} = \frac{50}{(0.2 * \langle n_g \rangle)^{0.44} \sqrt{V}}, \quad (23)$$

where V is the volume of the survey (or part of the survey under consideration) in $(h^{-1} \text{ Mpc})^3$, and n_g is the galaxy number density in $(h \text{ Mpc}^{-1})^3$. By performing this translation we have conservatively assumed that the error predicted on f by [17] was dominated by the measurement of $f\sigma_8^{\text{mass}}$, rather than the translation to f . The [17] formula has behaviour very close to Poisson with $\propto 1/N_{\text{gal}}$, consistent with the idea that we are not concerned with the scales on which we see galaxy pairs, but simply want amplitude information so all pairs count equally, and also assumes that we can recover information from both $P_{g\theta}$ and $P_{\theta\theta}$ [53]. This formulae is too simplistic to capture many of the dependencies, such as on galaxy bias and power spectrum shape, so we have performed a full Fisher matrix calculation. This validates this simple [17] formulae for reasonable values of galaxy bias, and galaxy power spectra. As our aim in this paper is to present the case for redshift-space distortions as a probe of dark energy models, the [17] formula is adequate for our purpose. We convert to calculate errors on f for Figs. 1 and 2 assuming that

$$\frac{\Delta f}{f} = \sqrt{\left(\frac{\Delta f \sigma_8}{f \sigma_8}\right)^2 + \left(\frac{\Delta \sigma_8}{\sigma_8}\right)^2}, \quad (24)$$

with $\sigma_8 = 0.82 \pm 0.03$, following the Λ CDM constraint from the 5-year WMAP data [37], and assume that the

same level of accuracy can be achieved at low redshift by the next generation of lensing experiments.

C. model comparison

Current and future constraints on $f\sigma_8^{\text{mass}}$ are compared with various models in Fig. 3. The models are all normalised to match the amplitude of fluctuations seen in the CMB by the 5-year WMAP experiment [37]. We see that future experiments will provide an order-of-magnitude improvement over current studies, and will provide constraints over a range of redshift from a single survey.

When comparing against models, we have not marginalised over parameters that are determined by the background, but instead fix parameters close to our sDE fiducial model in fitting to current geometrical constraint given by combination of WMAP, SN and Hubble key project. Fig. 3 therefore shows the differences between structure growth in the different models, rather than performing a full Likelihood test given current data. It shows what we can tell about structure formation if we have perfect information about the background expansion.

In detail, for DGP, we fix the distance to recombination at $z_{\text{iss}} = 1088_{-2}^{+1}$ through the measurement of the acoustic peak scale $l_A = 302_{1.4}^{+0.9}$ and its length calibration through the matter density $\Omega_m h^2 = 0.128 \pm 0.008$, and we fit the DGP cosmological parameter to the combination of SN and H_0 from Hubble Key Project. Open curvature is introduced to enhance the fit to data set. For cDE, we use the effective dark energy which makes the cDE geometrical factor exactly identical to the open DGP model used here. For IDE, we fix $\Omega_m h^2$ at its best value measured by WMAP, and we allow H_0 to be varied within 1- σ range of measured $H_0 = 72 \pm 8 \text{ km/sec/Mpc}$. Here we choose H_0 at the edge of upper bound, $H_0 = 80 \text{ km/sec/Mpc}$, at $\gamma = 0.3$. If γ becomes bigger than this value, then it is expected that it deviates significantly from the geometrical measurement as well as structural departure considered in this section.

In this paper we have followed standard convention and used σ_8^{mass} to normalise the matter power spectrum. The redshift-space distortion measurements actually constrain fluctuations on a range of scales larger than those probed by σ_8 , but this does not matter if we have a constant power spectrum shape. If the power spectrum shape is not constant, then the statistic used would have to be revised, and the full modelling of $P(k)$ included. This is beyond the scope of the current paper, and we assume a constant $P(k)$ shape. Here, we have assumed that the power spectrum of the initial fluctuations in the comoving gauge as measured by WMAP, has amplitude $\Delta_{\text{Cmb}}^2 = 2.4 \times 10^{-9}$. We assume that the time-dependent growth function of Φ is normalized to unity at the onset of matter domination and that the scale dependent transfer function is normalized to unity in the $k \rightarrow 0$ limit. For DGP and cDE models, we tune the acoustic

peak structure to be identical to sDE with same ω_m and ω_b and with fixing angular diameter distance to last scattering surface. For IDE, we do the same with the extra assumption that the earlier DE decay is negligible. This is a good approximation for small coupling limit used in this paper. The full treatment of the CMB in IDE models is beyond the scope of the current paper.

IV. FURTHER APPLICATIONS OF PECULIAR VELOCITY MEASUREMENTS

We now discuss additional cosmological applications that can be developed from peculiar velocity measurements. This is a development of previous work that considered constraints from observations of projected power spectra [8]. Here we assume that we have measurements of the growth of $P_{\theta\theta}$. We have a similar measurement from the combination of $P_{g\theta}$ and P_{gg} , but as this uses the continuity equation for baryons we treat this separately. First, we consider how a redshift dependent measurement of the amplitude of $P_{\theta\theta}$ can be used to reconstruct Ψ . We quantify this normalisation using σ_8^θ , defined as the rms fluctuations of θ averaged over spheres of radius $8 h^{-1} \text{ Mpc}$.

If we are able to probe the history of σ_8^{mass} , in addition to σ_8^θ , then we can complete the structure formation test. Measuring the derivative of σ_8^{mass} with respect to time would enable us to test the continuity equation by comparing it with σ_8^θ . This test eliminates many different theoretical models explaining cosmic acceleration, and is potentially more powerful than simply measuring only one of these quantities. Finally, the reconstructed Ψ created from σ_8^θ can be compared with Φ estimated from σ_8^{mass} , which will constrain the anisotropic stress.

Measuring the evolution of σ_8^{mass} is problematic because we cannot observe the mass directly. We could try to predict how galaxies trace the matter (e.g. [31, 32, 33, 34, 35]), or could measure this bias, for example using higher order statistics (e.g. [36]). Alternatively, we could use weak lensing measurements [7, 49, 50]. We expect that these methods will give constraints on bias at the percent level, by the time that redshift-space distortion measurements are obtained from the EUCLID experiment. Note that the weak-lensing constraints could themselves come from an imaging component of the EUCLID mission. For our proposed tests that require bias measurements, we therefore assume an expected uncertainty of $\Delta b/b \sim 0.02$. The models used match those described in Section III C.

A. Reconstruction of perturbed potential

If σ_8^θ can be measured with sufficient accuracy that its derivative can also be determined, then we can estimate Ψ from Eq. (3). The measured derivative of $\sigma_8^\theta(z)$ as a

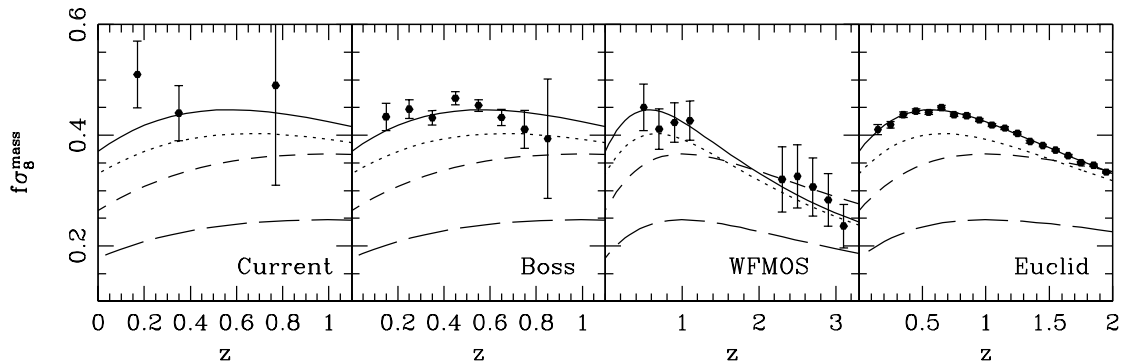


FIG. 3: The solid curve represents sDE, long-dash curve represents DGP, and dotted curve represents IDE. These models predict approximately the same background expansion, which is normalised at high redshift to match the fluctuations observed in the CMB. The left panel shows the current constraints discussed in the text. The three other panels show simulated data for BOSS, WFMOS and EUCLID-type experiments (see text for details).

function of redshift can be written

$$\frac{d\sigma_8^{\theta i}}{dt} = -\frac{H^i}{a} \frac{\sigma_8^{\theta i+1} - \sigma_8^{\theta i-1}}{2\Delta z}, \quad (25)$$

where i denotes each redshift bin. From this, we can construct an estimator of $\hat{\Psi}^i$ from

$$k^2 \hat{\Psi}^i = -H^i \frac{\sigma_8^{\theta i+1} - \sigma_8^{\theta i-1}}{2\Delta z} + \frac{H^i}{1+z^i} \sigma_8^{\theta i}. \quad (26)$$

We show estimates of how well future experiments will be able to reconstruct Ψ using this method in the top panel of Fig. 4. If there is no interaction between dark matter and dark energy, then $\langle \hat{\Psi} \rangle = \Psi$, since there is no change from the standard Euler equation. This offers a new way to probe the geometrical perturbation other than weak lensing experiment. Even with weak lensing measurements, it is interesting to have Ψ separately, because weak lensing probes the combination $\Phi - \Psi$.

B. Test on continuity equation

If we can measure the evolution of σ_8^{mass} and σ_8^{θ} simultaneously, then the continuity equation can be tested. The measured σ_8^{mass} at each redshift bin leads us to estimate its derivative in terms of time, which is defined by,

$$\frac{\sigma_8^{\delta i+1} - \sigma_8^{\delta i-1}}{2\Delta z} = \frac{\sigma_8^{\theta i}}{H_i}, \quad (27)$$

where i denotes the number of redshift bin. In the middle panel of Fig. 4, we show the estimated errors in constraining the continuity equation with EUCLID. The departure from the continuity equation of cDE model having the identical structure formation to DGP model (dash curve) is detectable. It means that MG models can be distinguishable from DE type model, i.e. modified gravity is detectable. The dotted curve representing IDE has

detectable departure from the continuity equation. This test will be a crucial future test for exotic DE models, but requires either galaxy bias to be fully understood or modelled. An alternative test using weak-lensing observations is possible.

C. Constraint on anisotropic stress

With the same assumption as in the previous subsection of an independent measurement on bias, we can extend the analysis to constrain anisotropic stress. The curvature perturbations are determined by

$$k^2 \Phi^i = 4\pi G_N a^2 \rho_m \delta_m^i, \quad (28)$$

so a measurement of the normalisation of the density field leads to a constraint on Φ^i . Using this measurement and the measurement in Section IV A, we are able to constrain anisotropic stress by comparing reconstructed Ψ^i and Φ^i . We show in the bottom panel of Fig. 4, that we are able to constrain the level of anisotropic stress predicted from DGP model.

V. CONCLUSIONS

One of the best ways of measuring this structure growth is to use observations of redshift-space distortions. This is an interesting and timely subject given current observations and those planned on a 10–20 year timescale [17, 51, 52]. In this paper we have reviewed the importance of redshift-space distortion measurements given that they provide a measurement of structure growth that is independent of galaxy density bias. We have argued that peculiar velocity measurements are best presented in terms of σ_8^{θ} , or $f\sigma_8^{\text{mass}}$ for models where the continuity equation holds. The independence from

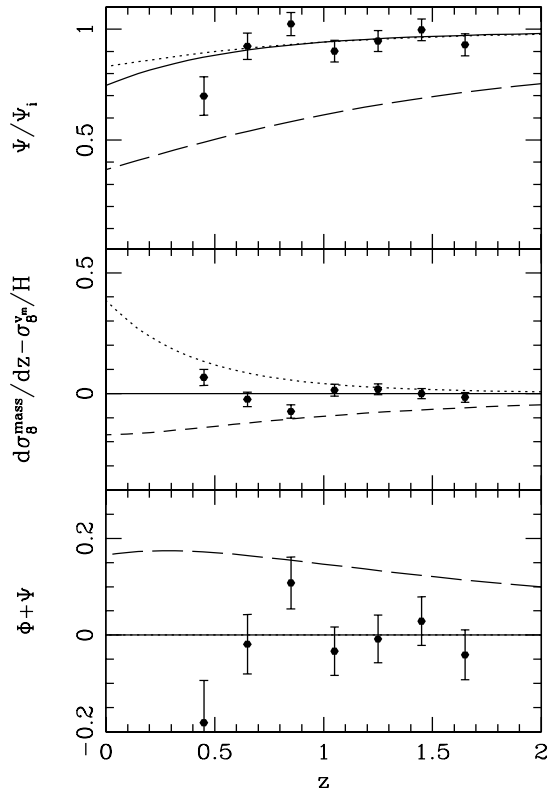


FIG. 4: Constraints on physical measurements that can be derived from a EUCLID type survey. The solid lines, long-dash lines, dashed lines and dotted lines are sDE models, DGP, cDE model and IDE model respectively. The top panel shows the reconstruction of Ψ from σ_8^θ , the middle panel shows the test of the continuity equation [30], and the bottom panel shows the constraint on anisotropic stress. The errors shown in this figure assume that we can recover σ_8^θ from both $P_{\theta\theta}$ and $P_{g\theta}$.

galaxy density bias has not been widely covered in previous literature. Most previous analyses have considered measuring β and $b\sigma_8^{\text{mass}}$, although there are some exceptions[13]. Although extremely simple, we have focused on the density bias independent constraint resulting from multiplying these together. The physical origin of such a constraint is that linear velocities, which scale with the derivative of the growth factor, depend only on the matter velocity field.

The primary conclusion from our work is that con-

straints on σ_8^θ or $f\sigma_8^{\text{mass}}$, are extremely good at helping to distinguish between the dark energy models that we reviewed in Section II. In fact, as we show in Fig. 1, these constraints are equivalent to similar percent measurements of f for some models of cosmic acceleration. They also have the simplicity of not having to model galaxy bias. The simple formula of [17] has been adapted to determine constraints on $f\sigma_8^{\text{mass}}$, and shows future constraints in Fig. 3. Although the [17] formula is simplistic, and might not be believed at the percent level, it shows that we can expect a huge step forwards in redshift-space distortion measurements with the next generation of surveys.

Going beyond simply obtaining a single measurement of σ_8^θ or $f\sigma_8^{\text{mass}}$, we have considered how the underlying perturbation evolution can be tested using peculiar velocity measurements. Peculiar velocity measurements are important because they can be used to reconstruct Newtonian potential Ψ which sources the dynamics of a galaxy given by Euler equation. Weak-lensing only measures Ψ in the combination $\Phi - \Psi$, so redshift-space distortions offer a complementary test of perturbations.

We have considered how peculiar velocities can be used to test the continuity equation, which is worthwhile since there are many theoretical models which fail to satisfy this relation. If dark energy couples to matter, then current constraints show that it must couple to the dark matter and not to baryonic material. The coupling of dark energy to dark matter modifies the Euler equation for dark matter, and breaks the equivalence principle between dark matter and baryon. This difference in free-fall breaks the continuity equation in which the peculiar velocity of matter is estimated using baryons, while we consider the growth of fluctuations in all matter. In addition, this test can tell if there is dark energy clustering which deepens the curvature potential well because we measure the peculiar velocity of the matter not of the total energy density. Finally we have considered how we can constrain the anisotropic stress by comparing Φ and Ψ , reconstructed from the density fields and peculiar velocity respectively.

Acknowledgments

We would like to thank Luca Amendola, David Bacon, Luigi Guzzo and Martin White for useful conversations. Y-SS and WJP are grateful to support from STFC.

[1] S. Perlmutter et al. (Supernova Cosmology Project), *Astrophys. J.* **517**, 565 (1999), astro-ph/9812133.
 [2] A. G. Riess, A. V. Filippenko, P. Challis, A. Clocchiatti, A. Diercks, P. M. Garnavich, R. L. Gilliland, C. J. Hogan, S. Jha, R. P. Kirshner, et al., *Astron. J.* **116**, 1009 (1998).
 [3] G. R. Dvali, G. Gabadadze, and M. Porrati, *Phys. Lett.*

B485, 208 (2000), hep-th/0005016.
 [4] S. M. Carroll, V. Duvvuri, M. Trodden, and M. S. Turner, *Phys. Rev.* **D70**, 043528 (2004), astro-ph/0306438.
 [5] A. Lue, R. Scoccimarro, and G. Starkman, *Phys. Rev.* **D69**, 044005 (2004), astro-ph/0307034;
 [6] M. Ishak, A. Upadhye, and D. N. Spergel, *Phys.*

- Rev. **D74**, 043513 (2006), astro-ph/0507184; Y.-S. Song (2006), astro-ph/0602598; L. Knox, Y.-S. Song, and J. A. Tyson, Phys. Rev. **D74**, 023512 (2006); K. Koyama, JCAP **0603**, 017 (2006) [arXiv:astro-ph/0601220]; J.-P. Uzan, Gen. Rel. Grav. **39**, 307 (2007), astro-ph/0605313; T. Chiba and R. Takahashi, Phys. Rev. **D75**, 101301 (2007), astro-ph/0703347; P. Zhang, M. Liguori, R. Bean, and S. Dodelson (2007), arXiv:0704.1932 [astro-ph]; L. Amendola, M. Kunz, and D. Sapone, JCAP **0804**, 013 (2008), 0704.2421; F. Schmidt, M. Liguori, and S. Dodelson, Phys. Rev. **D76**, 083518 (2007), 0706.1775; S. Wang, L. Hui, M. May, and Z. Haiman, Phys. Rev. **D76**, 063503 (2007), 0705.0165; E. Bertschinger, Astrophys. J. **648**, 797 (2006), astro-ph/0604485; W. Hu and I. Sawicki, Phys. Rev. **D76**, 104043 (2007), 0708.1190; W. Hu and B. Jain, Phys. Rev. **D70**, 043009 (2004), astro-ph/0312395; M. Ishak, Mon. Not. Roy. Astron. Soc. **363**, 469 (2005), astro-ph/0501594; V. Acquaviva, A. Hajian, D. N. Spergel, and S. Das (2008), 0803.2236; V. Acquaviva, C. Baccigalupi, and F. Perrotta, Phys. Rev. **D70**, 023515 (2004), astro-ph/0403654; B. Jain and A. Taylor, Phys. Rev. Lett. **91**, 141302 (2003), astro-ph/0306046; C. Schmid, J.-P. Uzan, and A. Riazuelo, Phys. Rev. **D71**, 083512 (2005), astro-ph/0412120; C.D. Porto and L. Amendola, Phys. Rev. **D77**, 083508 (2008).
- [7] B. Jain and P. Zhang (2007), 0709.2375.
[8] Y.-S. Song and K. Koyama (2008), 0802.3897.
[9] N. Kaiser, Mon. Not. Roy. Astron. Soc. **227**, 1 (1987).
[10] M. Colless et al. (2003), astro-ph/0306581.
[11] J. A. Peacock et al., Nature **410**, 169 (2001), astro-ph/0103143.
[12] E. Hawkins et al., Mon. Not. Roy. Astron. Soc. **346**, 78 (2003).
[13] W. J. Percival et al. (The 2dFGRS), Mon. Not. Roy. Astron. Soc. **353**, 1201 (2004), astro-ph/0406513.
[14] D. G. York et al. (SDSS), Astron. J. **120**, 1579 (2000), astro-ph/0006396.
[15] M. Tegmark et al., ApJ **606**, 702 (2004), arXiv:astro-ph/0310725.
[16] M. Tegmark et al. (SDSS), Phys. Rev. **D74**, 123507 (2006), astro-ph/0608632.
[17] L. Guzzo et al., Nature **451**, 541 (2008), 0802.1944.
[18] O. Le Fèvre et al., A&A **439**, 877 (2005), arXiv:astro-ph/0409135.
[19] B. Garilli et al. (2008), 0804.4568.
[20] D. J. Eisenstein, H.-j. Seo, and M. J. White (2006), astro-ph/0604361.
[21] O. Elgaroy et al., Phys. Rev. Lett. **89**, 061301 (2002), astro-ph/0204152.
[22] W. J. Percival, Astron. Astrophys. **443**, 819 (2005), astro-ph/0508156.
[23] K. Koyama and R. Maartens, JCAP **0601**, 016 (2006), astro-ph/0511634.
[24] I. Sawicki and S. M. Carroll (2005), astro-ph/0510364.
[25] M. Kunz and D. Sapone, Phys. Rev. Lett. **98**, 121301 (2007), astro-ph/0612452.
[26] L. Amendola, Phys. Rev. **D62**, 043511 (2000), astro-ph/9908023.
[27] D.F. Mota and C. van de Bruck, A.A. **421**, 71-81 (2004), astro-ph/0401504.
[28] L. Amendola, Phys. Rev. **D69**, 103524 (2004), astro-ph/0311175.
[29] K. Hagiwara et al. (Particle Data Group), Phys. Rev. **D66**, 010001 (2002).
[30] Y.-S., Song, K., Koyama, and R. Maartens, Prepared (2008).
[31] J. M. Bardeen, J. R. Bond, N. Kaiser, and A. S. Szalay, Astrophys. J. **304**, 15 (1986).
[32] S. Cole and N. Kaiser, Mon. Not. Roy. Astron. Soc. **237**, 1127 (1989).
[33] J. A. Peacock and R. E. Smith, Mon. Not. Roy. Astron. Soc. **318**, 1144 (2000), astro-ph/0005010.
[34] A. Cooray and R. K. Sheth, Phys. Rept. **372**, 1 (2002), astro-ph/0206508.
[35] U. Seljak, Mon. Not. Roy. Astron. Soc. **318**, 203 (2000), astro-ph/0001493.
[36] L. Verde et al., Mon. Not. Roy. Astron. Soc. **335**, 432 (2002), arXiv:astro-ph/0112161.
[37] E. Komatsu et al. (WMAP) (2008), 0803.0547.
[38] J. A. Peacock and S. J. Dodds, Mon. Not. Roy. Astron. Soc. **267**, 1020 (1994), astro-ph/9311057.
[39] R. Scoccimarro, Phys. Rev. **D70**, 083007 (2004), astro-ph/0407214.
[40] S. Hatton and S. Cole, Mon. Not. Roy. Astron. Soc. **296**, 10 (1998), arXiv:astro-ph/9707186.
[41] J. L. Tinker, D. H. Weinberg, and Z. Zheng, Mon. Not. Roy. Astron. Soc. **368**, 85 (2006), astro-ph/0501029.
[42] W. J., Percival, and M. White, (2008), arXiv:0808.0003.
[43] E. Regos and A. S. Szalay, Astrophys. J. **345**, 627 (1989).
[44] W. J. Percival and B. M. Schäfer, Mon. Not. Roy. Astron. Soc. **385**, L78 (2008), arXiv:0712.2729.
[45] M. Robert et al. (2007), astro-ph/0710.3970.
[46] A. Cimatti et al. (2008), astro-ph/0804.4433.
[47] www.dune-mission.net.
[48] K. Glazebrook, D. Eisenstein, A. Dey, and B. Nichol (2005), astro-ph/0507457.
[49] L. Amendola, M. Kunz and D. Sapone, JCAP **0804**, 013.
[50] V. Acquaviva et.al., (2008), arXiv:0803.2236.
[51] Y. Wang JCAP **0508**, 021.
[52] D. Sapone and L. Amendola, (2007), arXiv:0709.2792.
[53] M. White, Y.-S. Song and W.J. Percival, Mon. Not. Roy. Astron. Soc., *accepted*.
[54] Y.-S. Song, C. Sabiu and R. Nichol, *Prepared*.
[55] Y.-S. Song, Phys. Rev. **D77**, 124031 (2004), arXiv:0711.2513.